



HAL
open science

Quantitative measures in ISAR image formation based on Time-Frequency Representations

Jean-Christophe Cexus, Abdelmalek Toumi, Orian Couderc

► **To cite this version:**

Jean-Christophe Cexus, Abdelmalek Toumi, Orian Couderc. Quantitative measures in ISAR image formation based on Time-Frequency Representations. 2017 International Conference on Advanced Technologies for Signal and Image Processing (ATSIP) , May 2017, Fez, Morocco. 10.1109/ATSIP.2017.8075610 . hal-01670756

HAL Id: hal-01670756

<https://ensta-bretagne.hal.science/hal-01670756>

Submitted on 8 Jan 2018

HAL is a multi-disciplinary open access archive for the deposit and dissemination of scientific research documents, whether they are published or not. The documents may come from teaching and research institutions in France or abroad, or from public or private research centers.

L'archive ouverte pluridisciplinaire **HAL**, est destinée au dépôt et à la diffusion de documents scientifiques de niveau recherche, publiés ou non, émanant des établissements d'enseignement et de recherche français ou étrangers, des laboratoires publics ou privés.

Quantitative measures in ISAR image formation based on Time-Frequency Representations

Jean-Christophe Cexus, Abdelmalek Toumi, Orian Couderc

ENSTA Bretagne - Lab-STICC, UMR CNRS 6285

2, rue François Verny, 29806 Brest Cedex 9, France.

Email: {cexusje,toumiab}@ensta-bretagne.fr, orian.couderc@ensta-bretagne.org

Abstract—This paper proposes to adapt the Empirical Mode Decomposition Time-Frequency Distribution (EMD-TFD) to non-analytic complex-valued signals. This original method employs the Non uniformly Sampled Bivariate Empirical Mode Decomposition (NSBEMD) to design a filter in the ambiguity domain and clean the Time-Frequency Distribution (TFD) of the signal. This new approach is called NSBEMD-TFD. The suggested adaptation is used in the generation of Inverse Synthetic Aperture Radar (ISAR) image and compared to other Time-Frequency Representation (TFR) such as Spectrogram, Wigner-Ville Distribution (WVD)... Furthermore, two criteria to qualify TFD are adjusted to be perform on ISAR images generated by TFD. This method, called NSBEMD-TFD, and those criteria are tested on simulated data and also on data acquired from an anechoic chamber.

Keywords—Inverse Synthetic Aperture Radar, Image formation, Complex Empirical Mode Decomposition, Time-Frequency Analysis.

I. INTRODUCTION

In the ISAR imagery, a classic approach is built using Fourier Transform (FT). Nevertheless, to perform the FT it was supposed that the data as stationary signal, but that is not really true in reality. Indeed, the ISAR formation method is characterised by the movement of the target that induced the apparition of Doppler frequency making signals non-stationary. To deal with these temporal evolutions, a Time-Frequency analysis must be considered [1]–[3]. In recent years, a great deal of interest has been paid to transformations or processing that map the signal into its TFD [4]–[6].

Recently, Empirical Mode Decomposition (EMD) has been introduced by Huang *et al.* [7] for analyzing real data from non-stationary and non-linear processes. It is a local and fully data-driven method for the multi-scale analysis of non-linear and non-stationary real-world signals. Hence, this method is self-adaptive in contrast to the traditional methods where the basis functions are fixed [8]. The EMD is based on the sequential extraction of energy associated with various intrinsic time scales of the signal, called Intrinsic Mode Functions (IMF). The essence of the EMD is to identify the IMF in different time scales, which can be defined locally by the time lapse between two extrema of an oscillatory mode or by the time lapse between two zero crossings of such mode. The original EMD can only be applied to real-valued time series, so it is necessary to extend the EMD to the complex domain. Different methods have been proposed such as RIEMD (Rotation Invariant Empirical Mode Decomposition) [9], CEMD (Complex Empirical Mode Decomposition) [10],

BEMD (Bivariate Empirical Mode Decomposition) [11] or NSBEMD [12].

In the present work, NSBEMD method is used. In [12], the authors proposed an approach called Non uniformly Sampled Bivariate Empirical Mode Decomposition (NSBEMD), which differs from the original EMD in the way of getting the extrema and the envelopes. Indeed, this method is based on the idea of replacing the oscillation notion by a rotation notion. The complex signal was firstly projected to a several optimal directions to extract the maxima of the projection vector, and then connected these points forming the upper envelope. Repeat projecting the complex signal to different directions to obtain the envelopes. The NSBEMD algorithms finds a set of projection vectors distributed according to the principal direction, as opposed to uniform sampling performed by standard BEMD. In recent years, various methods based on EMD have received more attention in Radar field [13]–[16].

This paper is organized as follows. In section II, we briefly review the EMD-TFD algorithm of real-valued data, and describe an original method to the complex domain, called Non uniformly Sampled BEMD-TFD (NSBEMD-TFD) in order to handle the ISAR raw data. Section II gives also an overview of ISAR formation with Time-Frequency Representation and the method based on NSBEMD-TFD. We proposed also two criteria to qualify ISAR imagery based on TFR methods. Some simulations and comments are proposed in section III. Finally, the last section gives some conclusions and remarks.

II. METHOD DESCRIPTION

In this section, the NSBEMD-TFD algorithm is addressed. First, a brief introduction of EMD-TFD is presented and then, the NSBEMD-TFD algorithm is studied.

A. NSBEMD-TFD algorithm

In [17], [18], the authors proposed an interesting Time-Frequency method called EMD-TFD. The general principle rests on filtering the WVD interferences through the ambiguity function $A_x(\nu, \tau)$ of $x(t)$ is defined as [5]:

$$\iint_{-\infty}^{+\infty} A_x(\nu, \tau) e^{-2i\pi(\nu t + \tau f)} d\nu d\tau = WV_x(t, f), \quad (1)$$

where $WV_x(t, f)$ denotes the WVD of $x(t)$, $A_x(\nu, \tau)$ is the ambiguity function, τ is time-lag and ν is Doppler variable.

The EMD-TFD uses the EMD to design a filter $G(\nu, \tau)$ to clean the ambiguity domain $A_x(\nu, \tau)$ of $x(t)$. The adaptation

of the EMD-TFD to complex signal is done by using the NSBEMD instead of the original EMD. The NSBEMD-TFD principle is shown in Figure 1. In the case of this multiple-view TFD, the complex signals views are generated using the complex IMFs of NSBEMD (see **NSBEMD** box in Figure 1). The NSBEMD-TFD adaptively generates a set of filters functions (see **G** boxes in Figure 1) in the ambiguity domain of each IMF. So after computing the ambiguity function for each IMF, they are thresholded using an energy criterion [17] or a criterion on the maximal value of the function [18]. In the present work, this second method was used because it seems more applicable to ISAR image formation and permits a simplified implementation of the multiple-view approach [18]:

$$G_{IMF_i}(\nu, \tau) = \begin{cases} 1 & \text{if } |A_{IMF_i}(\nu, \tau)| \geq r \\ 0 & \text{otherwise} \end{cases}, \quad (2)$$

where $A_{IMF_i}(\nu, \tau)$ is the ambiguity domain representation of the i^{th} IMF, r is a user-defined threshold set between 0.2 and 0.5. Those thresholded functions (see **G** boxes in Figure 1) are combined by meaning them or by applying a logical OR (see **R** box represents the operation of filters combination in Figure 1). This combination provides a coarse filter that will be smoothed through a 2D window before cleaning the ambiguity function of the signal (see **X** operand in Figure 1). So, the NSBEMD-TFD process, $\Upsilon(t, f)$, is formalised as:

$$\Upsilon(t, f) = \iint_{-\infty}^{+\infty} G(\nu, \tau) A_x(\nu, \tau) e^{-2i\pi(\nu t + \tau f)} d\nu d\tau, \quad (3)$$

where $G(\nu, \tau) = \mathcal{R}_{i=1}^N [G_{IMF_i}(\nu, \tau)]$. In this work, the NSBEMD-TFD uses the arithmetic mean as the operator \mathcal{R} because it offers similar performance compared with other operators [18].

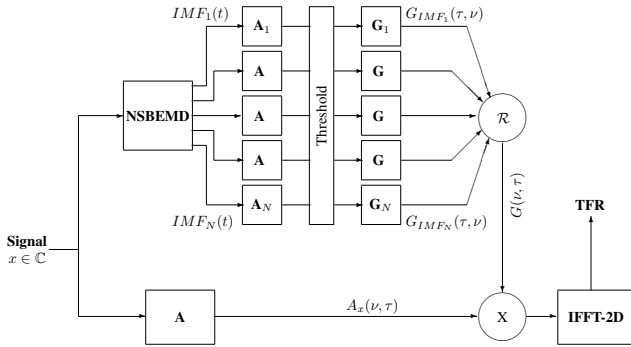


Fig. 1. Block diagram of the proposed algorithm [16].

B. Principle of ISAR Imaging based on NSBEMD-TFD

To compute a focused ISAR image of manoeuvring targets, a Time-Frequency Representation (TFR) is desirable. As in [3], the combination of TFD can be applied on ISAR image formation. On each range profile, a proposed multiple-view NSBEMD-TFD is performed to generate a time-Doppler representation. By combining the time-Doppler representations at range cells, we obtain a time-range-Doppler cube. Therefore, by replacing the 2-D Fourier Transform with TFR approach, a 2-D range-Doppler Fourier image frame becomes a 3-D time-range-Doppler images cube. By sampling the cube in time,

a sequence of 2-D range-Doppler images (frames) can be extracted. Each frame provides not only a clear image with superior resolution but also time-varying properties from one time to another. Figure 2 shows the radar imaging system based on the TFD technique [3].

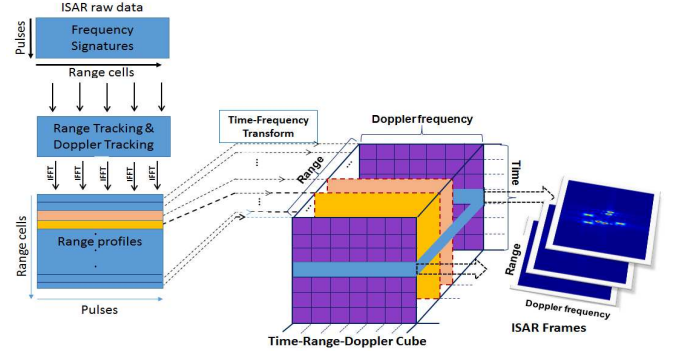


Fig. 2. Flowchart of ISAR image formation based on joint TFR [16].

C. Performance measures

In the aim to assess the quality of Time-Frequency methods in ISAR imagery, we adapt the criteria developed in [17]–[19] for ISAR image formation. The measures used to assess the performance of the ISAR image formation are based on the linear correlation coefficient, R_{id} , and the correlation coefficient between the ideal ISAR image using a truncated version of the ISAR image at a selected threshold, R_t . As a cube of data representing the image evolution through time is built with TFR those criteria are computed through time. The R_{id} is defined as:

$$R_{id} = \frac{\iint \rho(u, v) \rho_{id}(u, v) du dv}{\sqrt{\iint \rho(u, v)^2 du dv \iint \rho_{id}(u, v)^2 du dv}}, \quad (4)$$

where $\rho_{id}(u, v)$ is the ideal (theoretical) ISAR image, $\rho(u, v)$ is the ISAR image reconstructed by a Time-Frequency approach. R_{id} puts into relief the presence of interferences in the Time-Frequency Representation (the higher the interference, the lower the R_{id} correlation).

The second coefficient R_t is defined as:

$$R_t = \frac{\iint \rho_t(u, v) \rho_{id}(u, v) du dv}{\sqrt{\iint \rho_t(u, v)^2 du dv \iint \rho_{id}(u, v)^2 du dv}}, \quad (5)$$

where $\rho_t(u, v)$ is the same $\rho(u, v)$ is the ISAR image reconstructed but thresholded:

$$\rho_t(u, v) = \begin{cases} 1 & \text{if } \rho(u, v) \geq t_b \max[\rho(u, v)] \\ 0 & \text{otherwise} \end{cases}, \quad (6)$$

where t_b is a user-defined threshold selected as 0.90. R_t puts into relief the sharpness of the representation, and also if the components are enough intense. A ISAR image that is highly concentrated around the point scatterers (bright spots) of the moving target. To compute the ideal ISAR image through time, we use the theoretical points scatterers and the angular law employed to build data. One difference with the TFR version of these criteria is for the ideal image. For ISAR purpose we make each theoretical point have around the same dimension in cross-range as in range.

III. RESULTS

In this section, the ISAR imaging results for simulated and real data are provided to illustrate the effectiveness of the NSBEMD-TFD algorithm.

A. Simulated Data

The simulated dataset is composed of 3 point scatterers of equal reflectivity (Figure 3(a)). They are placed in a isosceles triangle configuration. The altitude of this triangle is 60cm and the length of the base is 33cm. This target is rotating from $[-30, 30]$ degrees with an angular step of 0.4 degree. So the raw data contains 153 recurrences of 101 ranges bins. We simulated a step-frequency radar with a central frequency of 10GHz, a bandwidth of 8GHz and 101 points of measures (*i.e.* a frequency step of 78 MHz). It should be noted that these parameters are also used to acquire experimental dataset with the anechoic chamber of ENSTA Bretagne, Brest (see subsection III-B). For all simulations, it should be noted that the representation of ISAR figures are first put on a logarithmic scale and then normalised.

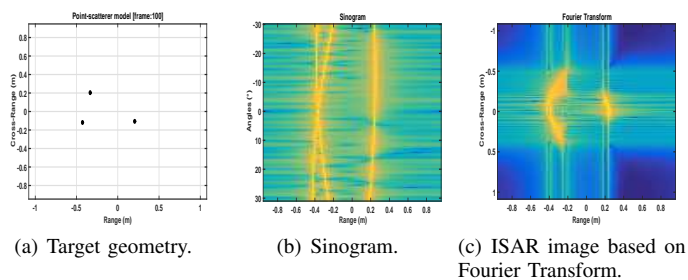


Fig. 3. Geometry, Sinogram and ISAR image of Synthetic target.

The ISAR imaging based on the conventional 2-D FT and sinogram are presented in the Figure 3(c) and Figure 3(b) respectively. Figures 4(a), 4(b), 4(c), 4(d) show one instantaneous ISAR imaging based on Spectrogram, Wigner-Ville Distribution (WVD), Smoothed Pseudo Wigner-Ville Distribution (SPWVD) and, NSBEMD-TFD respectively. The simulation results show that this ISAR formation based on TFD can improve the constructed image compared with the 2-D FT. In Figure 4(b), the blurring effects due to the cross-term interference associated with the WVD are evident. We can see that the ISAR image quality in Figure 4(c) seem better than in Figure 4(d). It should be noted here that these results also reflect several results publish in [16] (the authors used only simulated MIG25 model described in [3]).

Criteria R_t and R_{id} have been computed on these cubes and results are displayed in Figures 5(a), 5(b), 5(c), 5(d). Boxplots of R_{id} and R_t of various TFD are presented in the Figure 6(a) and 6(b) respectively. The Table I shows the median value of R_t and R_{id} for the cubes built with various TFD. However, R_t and R_{id} values are low. In fact, this is not a really issue with the sharpness of representations. These values are due to the fact that some points do not reach the level of ninety percent of the dynamic and then they are not represented in the thresholded image. The Spectrogram and WVD have the lowest values on these criteria. For WVD, it is explainable by the intense interferences in the ISAR image and then the low contrast between the background and the target representation. The R_t of the Spectrogram is due to the coarse representation (the sampling is different from the methods based on the WVD [5]).

The NSBEMD-TFD show the best performance. In fact, its R_t value is a consequence of the absence of high interferences in the NSBEMD-TFD representation.

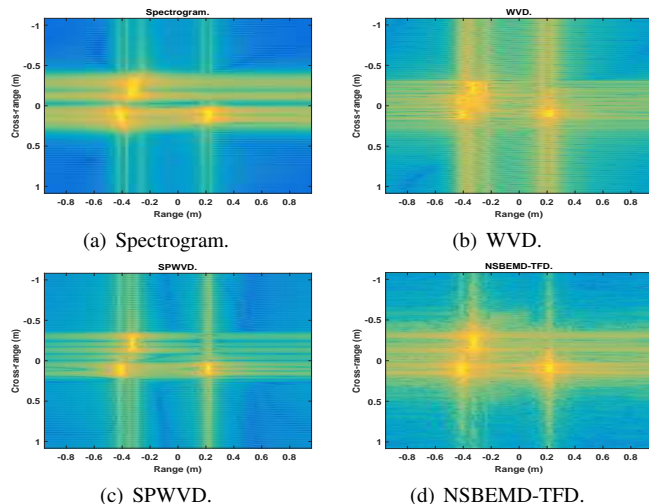


Fig. 4. Comparison of ISAR image based on TFR (frame 100).

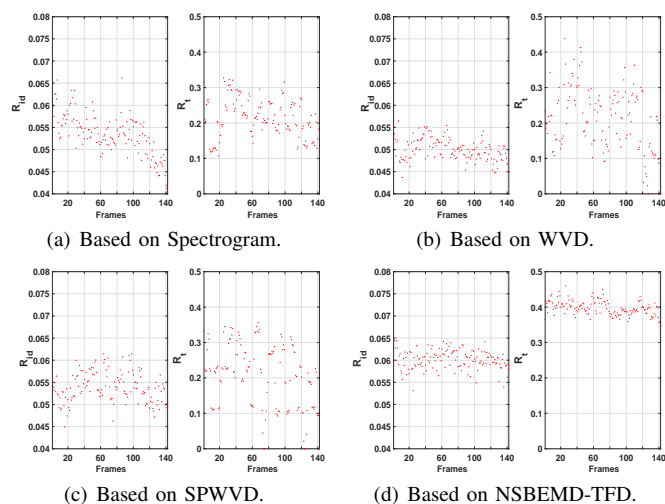


Fig. 5. Comparison of quality criteria R_t and R_{id} .

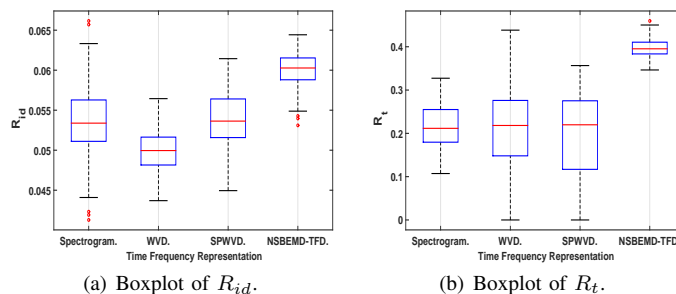


Fig. 6. Boxplot of quality criteria R_t and R_{id} for various TFD.

	R_{id}	R_t	$R = R_t + R_{id}$
Spectrogram	0.053	0.212	0.265
WVD	0.050	0.218	0.268
SPWVD	0.054	0.220	0.273
NSBEMD-TFD	0.060	0.395	0.456

TABLE I. MEDIAN VALUES OF R_{id} AND R_t FOR VARIOUS TFD.

B. Real Data

The target geometry and experimental parameters are identical to the one used in the numerical model given in the previous subsection III-A. The diameter of each ball is 4.5 cm. Hence, the experimental data from the target can be used to compare with the model's simulated results. Figures 7(a), 7(b) and, 7(c) show schematics of the experimental setup.

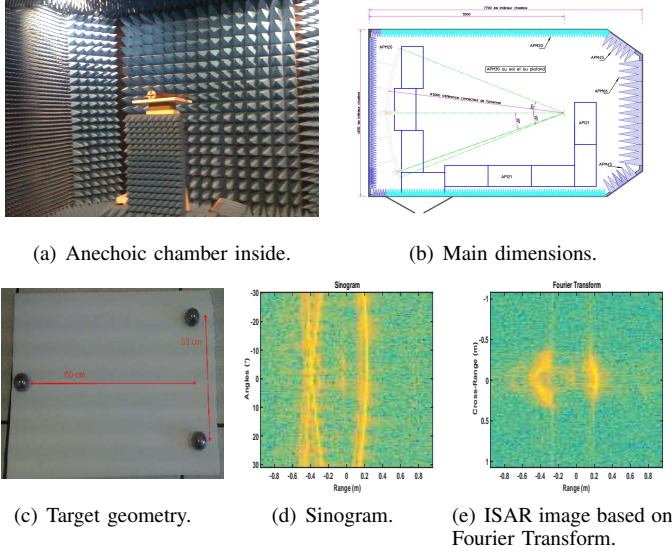


Fig. 7. System configuration, Sinogram and ISAR image of Real target.

Figures 8 show same ISAR images generated from same TFRs used in Figure 4. The same observations as for the Figure 4 can be made. For the NSBEMD-TFD, we have a better view of ISAR image. We can also notice that in the case of the WVD is filtering better than on simulated data and in general there is less interferences. This last statement can be due to the fact that we use only three balls.

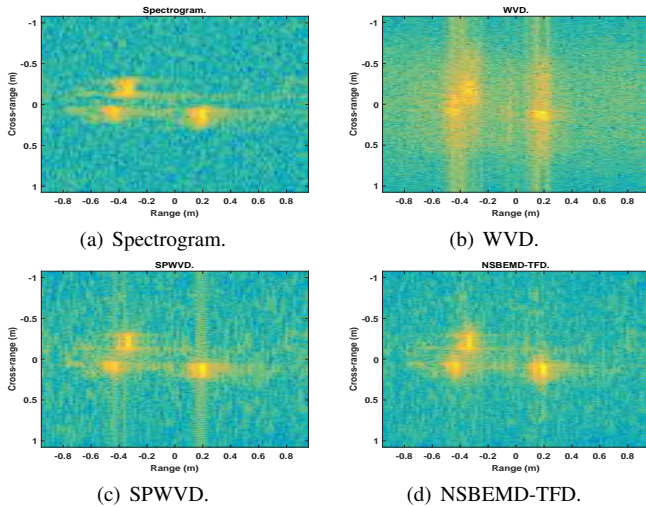


Fig. 8. Comparison of ISAR image based on TFR (frame 100).

Criteria R_{id} and R_t have been computed on these cubes and results are presented in the Table II and, boxplots displayed in the Figure 9(a) and 9(b) respectively. The NSBEMD-TFD shows the best performance. For R_{id} results are around the same low value. For R_t is high due to the strong contrast between the background and the points. In fact, R_t value is

a consequence of the absence of high interferences in the NSBEMD-TFD representation.

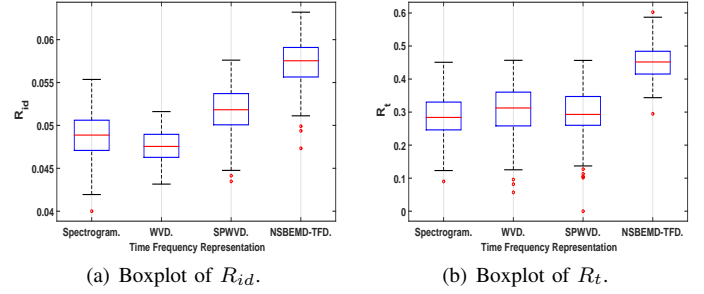


Fig. 9. Boxplot of quality criteria R_t and R_{id} for various TFD.

	R_{id}	R_t	$R = R_{id} + R_t$
Spectrogram	0.049	0.284	0.333
WVD	0.048	0.313	0.360
SPWVD	0.052	0.293	0.345
NSBEMD-TFD	0.058	0.452	0.509

TABLE II. MEDIAN VALUES OF R_{id} AND R_t FOR VARIOUS TFD ON REAL DATA.

IV. CONCLUSIONS

For ISAR imaging of a target, the echo signal in a range bin can be considered as a signal non-stationary and multi-components. In this paper, a novel algorithm for the ISAR imaging by the NSBEMD-TFD method is proposed. Then, the corresponding ISAR imaging algorithm based on NSBEMD-TFD is presented. We compare a variety of TFD methods to construct the ISAR imaging. Based on two measures R_{id} and R_t , the performance of the NSBEMD-TFD was compared to several TFD methods. The ISAR imaging results of synthetic and real data demonstrate the validity of the novel algorithm proposed in this paper. This approach has very good performance than traditional algorithms. However, the quality of ISAR imaging based on the NSBEMD-TFD technique is critical and a large class of data are necessary to confirm the results.

REFERENCES

- [1] V. C. Chen and H. Ling, *Time-Frequency Transforms for Radar Imaging and Signal Analysis*. Artech House Publisher, 2002.
- [2] I. Djurović, L. Stanković, V. Popović, M. Daković, and T. Thayaparan, "Time-Frequency Analysis for SAR and ISAR imaging," in *GeoSpatial Visual Analytics*, 2009, pp. 113–127.
- [3] V. C. Chen and M. Martorella, *Inverse Synthetic Aperture Radar Imaging - Principles, Algorithms and Applications*. SciTech Publishing, 2014.
- [4] L. Cohen, *Time-Frequency Analysis: Theory and Applications*. USA: Prentice Hall, 1995.
- [5] B. Boashash, *Time-Frequency Signal Analysis and Processing - A Comprehensive Reference*. Elsevier, 2003.
- [6] V. Corretja, E. Grivel, Y. Berthoumieu, J.-M. Quéllec, T. Sfez, and S. Kemkemian, "Enhanced Cohen class Time-Frequency Methods based on a Structure Tensor Analysis: Applications to ISAR Processing," *Signal Processing*, vol. 93, no. 7, pp. 1813–1830, 2013.
- [7] N. E. Huang, Z. Shen, S. R. Long, M. C. Wu, and *et al.*, "The Empirical Mode Decomposition and the Hilbert Spectrum for Nonlinear and Non-Stationary Time Series Analysis," *Proceedings of the Royal Society of London A: Mathematical, Physical and Engineering Sciences*, vol. 454, no. 1971, pp. 903–995, 1998.

- [8] G. Rilling, P. Flandrin, and P. Gonçalves, "Empirical Mode Decomposition as a Filter Bank," *IEEE Signal Processing Letters*, vol. 11, no. 2, pp. 112–114, 2004.
- [9] M. U. B. Altaf, T. Gautama, T. Tanaka, and D. P. Mandic, "Rotation Invariant Complex Empirical Mode Decomposition," in *Acoustics, Speech and Signal Processing, 2007. ICASSP 2007. IEEE International Conference on*, vol. 3, 2007, pp. 1009–1012.
- [10] T. Tanaka and D. Mandic, "Complex Empirical Mode Decomposition," *IEEE Signal Processing Letters*, vol. 14, no. 2, pp. 101–104, 2007.
- [11] G. Rilling, P. Flandrin, P. Gonçalves, and J. Lilly, "Bivariate Empirical Mode Decomposition," *IEEE Signal Processing Letters*, vol. 14, no. 12, pp. 936–939, 2007.
- [12] A. Ahrabian, N. U. Rehman, and D. Mandic, "Bivariate Empirical Mode Decomposition for Unbalanced Real-World Signals," *IEEE Signal Processing Letters*, vol. 20, no. 3, pp. 245–248, 2013.
- [13] B. Bjelica, T. Thayaparan, M. Dakovic, and M. Dakovic, "Complex Empirical Decomposition Method in Radar Signal Processing," in *Mediterranean Conference on Embedded Computing*, 2012.
- [14] J.-H. Park, W.-Y. Yang, J.-W. Bae, S.-C. Kang, and N.-H. Myung, "Extended high resolution range profile-jet engine modulation analysis with signal eccentricity," *Progress In Electromagnetics Research*, vol. 142, pp. 505–521, 2013.
- [15] B. A. H. Ahmed, J.-C. Cexus, and A. Toumi, "ISAR Image Formation with a Combined Empirical Mode Decomposition and Time-Frequency Representation," in *Proc. EUSIPCO'15*, 2015, pp. 1366–1370.
- [16] O. Couderc, J.-C. Cexus, F. Comblet, A. Toumi, and A. Khenchaf, "ISAR imaging based on the Empirical Mode Decomposition Time-Frequency Representation," in *International Radar Symposium 2016 - IRS2016, Krakow, Poland, (09-12 May)*, 2016, pp. 5–pages.
- [17] N. J. Stevenson, M. Mesbah, and B. Boashash, "A Time-Frequency Distribution based on the Empirical Mode Decomposition," in *Signal Processing and Its Applications, 2007. ISSPA 2007. 9th International Symposium on*, 2007, pp. 1–4.
- [18] —, "Multiple-View Time-Frequency Distribution based on the Empirical Mode Decomposition," *IET Signal Processing*, vol. 4, no. 4, pp. 447–456, 2010.
- [19] L. Rankine, N. J. Stevenson, M. Mesbah, and B. Boashash, "A Quantitative Comparison of Non-parametric Time-Frequency Representations," in *Signal Processing Conference, 2005 13th European*, 2005, pp. 1–4.